Ocean Sci. Discuss., 9, 2121–2151, 2012
www.ocean-sci-discuss.net/9/2121/2012/
doi:10.5194/osd-9-2121-2012

Ocean Science Discussions

The link between the Barents Sea and ENSO events reproduced by NEMO model

V. N. Stepanov, H. Zuo, and K. Haines

ESSC, University of Reading, Reading, UK

Received: 25 April 2012 – Accepted: 7 May 2012 – Published: 25 May 2012

Correspondence to: V. N. Stepanov (vlnst@hotmail.co.uk)

Published by Copernicus Publications on behalf of the European Geosciences Union.

Abstract

An analysis of observational data in the Barents Sea along a meridian at 33°30′ E between 70°30′ and 72°30′ N has reported a negative correlation between El Niño/La Niña-Southern Oscillation (ENSO) events and water temperature in the top 200 m: the temperature drops about 0.5 °C during warm ENSO events while during cold ENSO events the top 200 m layer of the Barents Sea is warmer. Results from 1 and 1/4-degree global NEMO models show a similar response for the whole Barents Sea. During the strong warm ENSO event in 1997–1998 an anticyclonic atmospheric circulation is settled over the Barents Sea instead of a usual cyclonic circulation. This change enhances heat loses in the Barents Sea, as well as substantially influencing the Barents Sea inflow from the North Atlantic, via changes in ocean currents. Under normal conditions along the Scandinavian peninsula there is a warm current entering the Barents sea from the North Atlantic, however after the 1997–1998 event this current is weakened.

During 1997–1998 the model annual mean temperature in the Barents Sea is decreased by about 0.8 °C, also resulting in a higher sea ice volume. In contrast during the cold ENSO events in 1999–2000 and 2007–2008 the model shows a lower sea ice volume, and higher annual mean temperatures in the upper layer of the Barents Sea of about 0.7 °C.

An analysis of model data shows that the Barents Sea inflow is the main source for the variability of Barents Sea heat content, and is forced by changing pressure and winds in the North Atlantic. However, surface heat-exchange with atmosphere can also play a dominant role in the Barents Sea annual heat balance, especially for the subsequent year after ENSO events.

1 Introduction

Serreze et al. (2007) showed that the Barents Sea in spite of its small size is a main reservoir of Arctic Ocean seasonal heat storage: with an area of about 14 % of the Arc-

OSD
9, 2121–2151, 2012

tic Ocean, more than 50 % of the total arctic heat loss occurs in the Barents Sea. This is because the southern Barents Sea remains open during all year, while other Arctic Seas are covered by sea ice that prevents further cooling. The warm and relatively saline water entering the Barents Sea from the North Atlantic keeps the subsurface layers warm through into November despite cooling of the surface waters above. The final winter mixed layer depth in the Barents Sea reaches 250 m compared to only ∼100 m depth elsewhere in the Arctic and therefore there is a very strong seasonal cycle in heat storage. It is natural therefore that any strong interannual anomalies, in either the surface heat loss or the inflow of heat from the North Atlantic, will have a signal in the heat storage and Barents sea temperatures for periods of up to a year at least.

A recent analysis of observational data (for nearly a century) in the Barents Sea along a meridian at 33°30′ E between 70°30′ and 72°30′ N (Byshev, 2003) showed negative correlation between ENSO events and water temperatures in the top 200 m: the temperature drops about 0.5 °C during warm ENSO events while the top 200 m layer is warmer (also by about 0.5 °C) during cold ENSO events. During warm ENSO events atmospheric teleconnections lead to an anticyclonic atmospheric circulation pattern (higher atmospheric pressure) settling over the Barents Sea, instead of the more usual cyclonic conditions observed during winter months. These ocean mean temperature differences are seen in both summer and winter months.

This paper presents the results of a numerical ocean model based reanalysis of the changing conditions of circulation and temperatures in the Barents Sea, in the presence of changing atmospheric forcing anomalies. Section 2 briefly introduces the NEMO model and forcing data. Section 3 describes the assimilation method used and the design of the numerical experiments analysed. Section 4 looks at atmospheric circulation over the Barents Sea during cold and warm ENSO events, and the corresponding changes in the model ocean circulation are discussed. Section 5 shows the model relationships/correlations between atmospheric and ocean characteristics, such as atmosphere and ocean temperatures, sea level pressure, and ocean heat content etc.

OSD
9, 2121–2151, 2012

Section 6 provides some discussion and conclusions about the link between the atmospheric and ocean processes.

2 Model description

The numerical model used is the NEMO coupled ice-ocean model (Madec, 2008) version 2.3, based on the OPA9 code (Madec et al., 1998) and the LIM2.0 sea ice model (Louvain sea Ice Model: Fichefet and Maqueda, 1997; Goosse and Fichefet, 1999), which is a dynamic-thermodynamic model specifically designed for climate studies. The ocean model is a primitive equation z-level model making use of the hydrostatic and Boussinesq approximations. The model employs a free surface (Roullet and Madec, 2000) with partial cell topography (Adcroft et al., 1997). The version used here has a tri-polar "ORCA" grid with 46 levels in the vertical, with thicknesses ranging from 6 m at the surface to 250 m at the ocean bottom. The model configurations are (i) a global 1° resolution with a tropical refinement to 1/3° (ORCA1) and (ii) a global 1/4° resolution (ORCA025) with horizontal resolution 27.75 km at the equator, 13.8 km at 60° N, down to 10 km in the Arctic Ocean. These configurations have been developed through the DRAKKAR Consortium (Barnier et al., 2007) and use model parameter settings as defined in Barnier et al. (2006) and Penduff et al. (2010). The model employs an energy-enstrophy conserving momentum advection scheme (Barnier et al., 2006) and a Laplacian diffusion. Horizontal viscosity is parameterized with a Laplacian operator. Additionally the ORCA1 model makes use of the Gent and McWilliams (1990) mixing parameterization. Vertical mixing is parameterized using a one-equation turbulent kinetic energy scheme (Blanke and Delecluse, 1993). More details may be found in Barnier et al. (2006), and Penduff et al. (2007).

Surface atmospheric forcing for the period 1989–2008 is obtained from ECMWF ERAInterim 6 hr reanalysis (Simmons et al., 2007; Dee and Uppala, 2009). The ERAInterim reanalysis provides 10-m wind, 2-m air humidity and temperature, to compute 6-hourly turbulent air/sea and air/sea-ice fluxes using the bulk formula proposed by Large

OSD
9, 2121–2151, 2012

and Yeager (2004). Downwelling short and long wave radiative fluxes and precipitation are also provided by ERAInterim. While biases in radiation and precipitation fields are inevitable we find that the heat and freshwater budgets of the NEMO model are able to come into global balance with the ERAInterim forcing without further modifications being made (M. Valdivieso, personal communication), see also Haines et al. (2012).

3 Description of numerical experiments

The experiments described in the paper are summarized in Table 1. All ORCA1 experiments (CTL1 and ASSIM1) were initialised with a cold-start in 1989 using the World Ocean Atlas 2005 (WOA05) climatology (Boyer et al., 2006) initial conditions and spun-up through to the end of 2008, using ERAInterim forcing. A control CTL1 experiment (with 1° resolution) was run free through 1989–2008, while the ASSIM1 (1°) experiment assimilated hydrographic data as in (Smith and Haines, 2009), using the ENACT/ENSEMBLES EN3v2.1 data, (Ingleby and Huddleston, 2007). The assimilation run at 1/4° resolution is designated UR025.3, and covers the period 1989–2008, also using ERAInterim forcing, but initiated from a 1/4° run called G70 from 1958–1989, driven by the hybrid interannual forcing DFS3 described in detail in Brodeau et al. (2009). This blends 6-hourly 10-m atmospheric surface variables from the ERA40 reanalysis (turbulent fluxes) with daily or monthly satellite-derived radiative fluxes and precipitation. The assimilation period from 1989–2008 again used hydrographic data assimilation with ENACT/ENSEMBLES EN3v2.1 (Ingleby and Huddleston, 2007).

The data assimilation method of (Haines et al., 2006; Smith and Haines, 2009), previously implemented within NEMO, was used for the assimilation. Referred to as the $S(T)$ scheme this is a two step sequential scheme for hydrographic data based on Optimal Interpolation. Temperature profiles (T) are assimilated along with a salinity balancing increment (Troccoli and Haines, 1999) to maintain the model's watermass properties (i.e. temperature-salinity relationships) in the absence of salinity data. In the second step salinity profiles (S) are assimilated along isotherms (i.e. $S(T)$, see Haines

OSD
9, 2121–2151, 2012

et al., 2006). With the $S(T)$ increments being spread along isotherms this means that corrections to a particular water mass do not influence adjacent water masses, which may have uncorrelated errors. The scheme has been thoroughly tested and is used as part of the ECMWF system 3 ocean reanalysis, Balmaseda et al. (2008). The assimilation increments are determined at the end of each five day period and a variant of the (Bloom et al., 1996) incremental analysis update method is used to add these increments evenly over the subsequent day.

Conventional spatial covariance scales defined in Carton et al. (2000) were used to spread out the increments to be made to the model T and S properties around the region where observation-model differences are detected. These scales were determined by Carton et al. (2000) by comparing anomaly decorrelation scales from pairs of in situ temperature observations (the zonal length scale varies from 450 km at the equator to 375 km in midlatitudes, and the meridional length scale varies from 250 km at the equator to 375 km in midlatitudes).

Since the 1989–2008 period is too short to include many ENSO events, we have also used the ORCA025-G70 1/4° horizontal resolution eddy-admitting 1958–2004 global ocean/sea-ice simulation implemented and performed by the DRAKKAR group (2007) as part of a wider numerical simulation database. This global simulation was the same used to initialize UR025.3 in 1989 and is driven without data assimilation over the whole 1958–2004 period by the hybrid interannual forcing DFS3 described in detail in Brodeau et al. (2009).

4 Interannual variation in the Barents Sea during ENSO events

Figure 1a shows the top 200 m annual averaged temperatures in the region of the Barents Sea (Fig. 1b) from 3 different model experiments (black, green and red lines). Also shown are the sea ice volume from the UR025.3 experiment and the NINO3 index (using the temperature scale).

OSD
9, 2121–2151, 2012

There are three strong ENSO events: a warm event in 1997–1998 and two cold events in 1999–2000 and 2007. During the warm ENSO in 1997–1998 the annual mean model temperatures in the Barents Sea clearly decrease (achiving about 0.8 °C over the next year) for all model runs, and a higher sea ice volume in UR025.3 is also clear. In contrast in 1999–2000 and 2007–2008 the model shows higher than normal annual mean temperatures in the Barents Sea, of ∼0.7 °C, and lower sea ice volumes. While these only represent a small number of events we can take them as case studies for the local changes in the Barents Sea heat budget that accompany the changes in regional atmospheric forcing in these ENSO periods. These cool and warm Barents Sea events also appear to last over a 2 year period with the maximum change in sea ice volume being observed in the second year.

Temperature variability from the 1° and 1/4° models look similar, however the 1° models overestimate the average temperature when compared to observations (see, e.g., Smedsrud et al., 2010), with the 1° assimilation giving the highest temperatures. Both the 1° models CTL1 (3.8 Sv) and ASSIM1 (3.9 Sv) also overestimate the volume inflow into the Barents Sea compared to inverse model results (3.5 Sv) (Tsubouchi et al., 2011) which probably explains the higher Barents Sea temperatures. The higher model resolution in UR025.3 produces the best estimation of the Barents Sea inflow (3.4 Sv) and therefore has more realistic upper ocean temperatures. The variability however does not substantially depend on model resolution (the standard deviation of annual mean temperatures is ∼0.4 °C for CTL1 and UR025.3 experiments and ∼0.5 °C for ASSIM1), and we therefore assume the mechanisms of variability are not sensitive to resolution.

Figure 2a and b shows ERAInterim sea level pressure anomalies (from the 1989–2008 mean), for the northern winter period JFM (i.e., January, February and March) during the 1998 warm and the 2000 cold ENSO events. During JFM 1998 global atmospheric teleconnections lead to higher atmospheric pressure (Fig. 2a), and hence lower air temperatures over the Barents Sea, while during JFM 2000 lower atmospheric pressure (Fig. 2b), lead to warmer air temperatures over the Barents Sea. These con-

OSD
9, 2121–2151, 2012

ditions lead to higher than averaged over 1989–2008 period heat loss over the Barents Sea in 1998 and lower heat losses in 2000 in all the model runs (e.g. Fig. 2c–d).

Figure 3a and b shows wind stress anomalies for January–March 1998 and 2000 over the North Atlantic and the Barents Sea. This leads to a change in the Barents Sea mean currents. Figure 3c–f shows the top 200 m averaged current velocity anomaly from the CTL1 (Fig. 3c, d) and UR025.3 (Fig. 3e, f) experiments for January–March of 1998 (Fig. 3c, e) and 2000 (Fig. 3d, f). Under normal conditions along the Scandinavian peninsula there is a warm current entering the Barents Sea from the North Atlantic, however in JFM 1998 this current is much weaker, which therefore decreases the heat entering the Barents sea from the North Atlantic. The flow through the Kara Gate (the strait between Vaygach and Novaya Zemlya) reverses direction from 2000 to 1998. This also leads to colder conditions in 1998: the transport of the warm North Atlantic water is decreasing while more cold waters from the Kara Sea are entering the Barents Sea. Similar changes are obtained for the UR025.3 experiment. Figure 4 shows the monthly anomalies of volume and heat inflow into the Barents Sea after removing the seasonal cycle (from the UR025.3 experiment). We clearly see that there is high correlation between volume and heat inflow in the Barents Sea, and we will show that this is the critical variability for controlling interannual changes in Barents Sea heat content.

Thus we see that the change in atmospheric circulation can lead to changes in both surface heat loss over the Barents Sea and heat entering from the North Atlantic. The relative importance of these mechanisms is discussed in the next section.

5 Heat budget variability in the Barents Sea

Normalised seasonal cycle variability over 1989–2008 from the UR025.3 experiment is shown for the Barents Sea heat budget terms along with vertical structure, in Fig. 5. Heat is transported into the Barents Sea throughout the year but particularly in late autumn to early winter (black, peaking in December with a minimum in May) by ocean currents from the North Atlantic. In summer shortwave radiation adds heat to the Barents

OSD
9, 2121–2151, 2012

Sea (red, peaking in June) and heat is lost by latent, sensible and long wave radiation in winter (see, e.g., Smedsrud et al., 2010). The Barents Sea total heat content (green, the top 200 m mean temperature) shows every sign of being controlled primarily by the surface shortwave cycle, being 90° out of phase with the surface forcing.

The heat content of the deeper layers, and the deep vertical structure of the Barents Sea is however more clearly related to the heat inflow from the Atlantic, with the depth of the 1 °C isotherm (blue) remaining shallow from February through June and only deepening substantially after August when the ocean inflow from the North Atlantic (black) reaches its peak. The minimum temperature in the 130–320 m layer (dashed blue) also characterizes the impact of the Barents Sea heat inflow: the dashed blue and black lines vary almost in phase with each other. The January–April decrease of the Barents Sea heat inflow, accompanied by surface heat losses, leads to a cooling of this deep ocean layer.

The spring and summer warming due to absorption of incoming short wave radiation forms a sharp and shallow pycnocline in the Barents Sea. It substantially makes difficult the heat- and salt- exchanges of deep and upper layers. As a result the 1 °C isotherm is shallower (in comparison with its mean value) until August since the heat transport from the North Atlantic is low during this time. Only after August the 1 °C isotherm is deepening that is caused by the increase of the Barents Sea heat inflow.

As follows from Fig. 6, winter months (from January to March, when the main cooling occurs) and the period of July–August (when maximal ocean warming is observed) give the main contribution to annual values of the net surface flux (green line), while almost for each month there are strong correlations between annual heat transported by the Barents Sea inflow and its time series corresponding to each month (red). The North Atlantic heat transport during cold periods compensates winter cooling of the Barents Sea, but this heat transported from April to July (though these values are smaller than during cold periods, Fig. 5) can be accumulated by the Barents Sea water resulting in the formation of either positive or negative summer heat content anomalies. These anomalies can influence the state of the Barents Sea during the following cold season.

OSD
9, 2121–2151, 2012

Therefore high correlation between the inflow and the Barents Sea temperature has been found by many authors (e.g., Loeng et al., 1997; Dickson et al., 2000; Furevik, 2001).

Figure 7 looks at the interannual variability in Barents Sea mean temperatures in relation to the surface heat fluxes and the heat inflow from the Atlantic during the ERAInterim period from UR025.3 run. There is a close correspondence between cold (warm) conditions in the Barents Sea (red) and the lower (higher) Barents Sea inflow (black) in Fig. 7. However there is no obvious connection between the Barents Sea temperature and the net Barents Sea annual mean surface heat flux (green). It can also be seen that strong ENSO events (blue dashed) are negatively correlated with the Barents Sea inflow. The correlation between the annual Barents Sea top 200 m temperature and heat inflow time series is about $C_{TF} \approx 0.7$ and approximately the same correlation coefficient is obtained when the Barents Sea inflow variability leads by 1 year the temperature changes (statistically significant at 95 % level). However the annual net Barents Sea surface heat flux variability lags by 1 year the annual Barents Sea temperature variability, with a statistically significant negative correlation coefficient of $C_{TH} \approx -0.6$. Similar correlations of the annual Barents Sea temperature with the Barents Sea inflow and the net surface heat flux time series are obtained for ORCA025-G70 model data: $C_{TF} \approx 0.7$ and $C_{TH} \approx -0.5$.

Figure 8 presents the normalized April–December mean time series of NINO3-index (blue), and time series of the averaged Barents Sea heat content (green) and heat inflow (red) obtained by averaging monthly data from April to March of the subsequent year. Since the main teleconnections with ENSO (achiving maximal development phase in December) are observed in the beginning of the next year, so the different averaged periods were chosen here. The black line shows time series of the net surface flux calculated similar to red time series, but scaled by the standard deviation of the Barents Sea heat inflow, so as to obtain these two time series on the same scale for the global Barents Sea heat balance.

OSD
9, 2121–2151, 2012

Though Fig. 8 shows some reverse correspondence between major number of peaks and troughs of NINO-index with ones of the temperature curve, however only for 3 of 7 strong ENSO events (1 warm: 1982 and 2 cold: 1973 and 1984, when the values of NINO3-index deviate more than 1 standard deviation) a negative correlation with the Barents Sea temperature is observed in the same year. While for two warm (1987 and 1997) and two cold (1988, 1999) ENSO events NINO-index leads the Barents Sea temperature variability with lag of 1 year for warm and 2 years for cold ENSO events, respectively. The ENSO events before 1972 varied very frequently (they have been altered every 1–2 years), therefore likely did not lead to substantial the Barents Sea temperature variability: the cooling due to previous ENSO was compensated by warming by the subsequent ENSO event, and vice versa.

For 5 cases (1982, 1987 – warm, and 1973, 1988, 1999 – cold) of these 7 strong ENSO the Barents Sea heat content anomaly are due to corresponding heat inflow extrema. For 2 other cases (1984 and 1997) a relationship with Barents Sea heat content is found but not with heat inflow. The warm 1997 ENSO event results in the Barents Sea cooling during the next year that is caused by higher the Barents Sea heat loss through its surface in comparison with the low heat inflow during the period of 1997–1998. The cold 1984 ENSO looks like outline: the values of both the heat inflow and the net surface flux are near averaged ones. However this event has occurred immediately after strong warm ENSO in 1982–1983. Likely the interaction between the atmosphere and ocean during the period 1982–1983 could lead the case when the heat inflow into the Barents Sea and the net surface flux have been changed in the same phase (Fig. 8) leading to higher the Barents Sea temperature in 1984.

Thus in more than 70 % cases (for 30 year period) a negative correlation between temperature and ENSO events is due to the Barents Sea heat inflow variability, though in some cases the net surface flux change at interannual scales also can have impact on the Barents heat balance. According to NEMO model the values of the Barents Sea heat content averaged from April to March of the subsequent year are positively correlated with the similar time series of the Barents Sea inflow (correlation coefficient

OSD
9, 2121–2151, 2012

is about 0.9) and negatively with the net surface flux (with correlation of about −0.9). Also there is negative correlation between the net surface flux and the Barents Sea inflow with coefficient of about −0.8.

Anyone can argue that it is very difficult to make the statement, which is saying that ENSO events can cause Barent Sea temperature changes in the same year, or in the subsequent year, or even after 2 years when another ENSO event may already be happened. However, if we consider ENSO events as a consequence of the change of the global meridional atmospheric circulation, so the suggestion about the link between the high and low latitudes can be justified. This link between the tropics and the high latitudes can be explained by the result of the interaction between the tropics and the mid latitudes that then influence the high latitudes. Warming (cooling) of the upper ocean layer in the tropics (which can be related, for example, to the seasonal cycle) leads to an increase (decrease) in the warming of the troposphere in the zone of atmospheric mass upwelling in the tropics (the Pacific Ocean is the largest ocean and its contribution to these changes is maximal). This means that a warmer (colder) upgoing air from the tropical zone is transported by the Hadley circulation cell to the region of downgoing air masses of the subtropics, which slows down (accelerates) the air motion in the downgoing branch of the Hadley cell and then leads to weakening (intensification) of the wind in the mid latitudes, which then lead to similar changes in the high latitudes. Particularly for the Barents Sea, as we will see later, the weaker wind in the high latitudes means the lower heat inflow, and hence its lower heat content. The next paragraph confirms the hypothesis about of the possible link between processes occurred in the low and high latitudes.

Around 1960s, Bjerknes indicated on links between ENSO and the Southern Oscillation described by SOI-index (fluctuations in the difference of the surface air pressure anomalies between Tahiti (17°52′ S) and Darwin (12°25′ S)), and so far the SOI-index is used as a good predictor of ENSO events. Figure 9a shows 1989–2008 correlations of zonally averaged monthly sea level pressure (SLP) with SOI-index taken with negative sign. We clearly see seasonality and that SOI-index leads the SLP change in low

OSD
9, 2121–2151, 2012

latitudes. However, as Fig. 9b–d demonstrates, the change of the zonal SLP occurs in phase with the change of the meridional gradient of the SLP, and, likely the meridional gradient change of the SLP is primary source of the SLP variability in the low latitudes that then in its turn, results in to the next SLP change in the tropics in the zonal direction (Fig. 9a). After removing of seasonal cycle and implementation of low-pass filtering with periods longer than 18 months correlation between SOI-index and the zonally averaged sea level pressure difference between 17° and 12° S (Fig. 9d) is about −0.6. Thus, it is likely that the development of ENSO events is due to the global meridional atmospheric circulation change that can affect high latitudes too: the stronger these changes, the stronger effect can be seen both in the low and high latitudes. Since the interaction between the tropics and high latitudes depends on the stochastic processes, which always occur during the interaction between the atmosphere and the ocean, therefore it is difficult to reveal a definite link between the low and high latitudes immediately: some interaction delay between these latitudes can be due to the strength of current and previous ENSO events.

Figure 10 also demonstrates that the Barents Sea inflow variability and thermal conditions of the Barents Sea substantially depend on ENSO events presenting correlations in April–July mean ERAInterim sea level pressure with (a) April NINO3-index and (b) April–July Barents Sea mean inflow, for 1989–2008, calculated from UR025.3 model data. We used here NINO3-index averaged for April as an early possible predictor for ENSO events, since the annual NINO3-index strongly correlates with its time series corresponding to each month from April to December (Fig. 6).

The anticorrelations are clear to see and in particular in Fig. 10b shows the stronger winds blowing inflow towards the Barents Sea. The Barents Sea inflow is correlated with changes in the westerly winds in the North Atlantic, represented by pressure differences between N Western Europe and Spitsbergen, ΔPa, (the regions are marked by black crosses on Fig. 10a–b). Figure 10c shows monthly values of the Barents Sea inflow and the ΔPa time series. Correlation between the Barents Sea inflow and ΔPa is ~0.8 and statistically significant at the 95 % level. There are some similarities with the

OSD
9, 2121–2151, 2012

results of Hughes and Stepanov (2004) who found correlation between the sea level variability in the northern polar seas and pressure differences between Greenland and southern Scandinavia (note that they used the NCEP reanalysis pressure distributions rather than ERAInterim).

The above discussions show that heat storage in the previous year can influence the Barents Sea heat balance during the next year. We can explain this by a dominant role of the Barents Sea inflow from the North Atlantic: cooling during cold periods is restricted by the Barents Sea ice formation in the upper layers (i.e. when the temperature achieves freezing point the Barents Sea is covered by the sea ice and it stops loosing heat). While in the deeper layers the heat supply from the North Atlantic (that has maximal values during that time, Fig. 5) is continued. April–June Barents Sea inflow from the North Atlantic leads to the heat accumulation in deep layers that results in the formation of either positive or negative heat content anomalies before the next cold period. These anomalies can influence the heat lost during the next cold season: the warmer the sea water temperature and deeper the layer of this water, the higher heat loss during the subsequent cold period. The negative correlation between the averaged for the period of April–March net surface flux and the top 200 m averaged Barents Sea temperature time series shown early (−0.9) and the results presented on Fig. 11 confirm this. This figure shows normalized on their standard deviations anomalies (after subtraction of seasonal cycle) of the depth of 1 °C isotherm (blue), the averaged Barents Sea temperature (green), the Barents Sea heat inflow (black) and the net surface flux (red) after applying a low-pass filter with periods longer than 24 months. We clearly see that (if we discard the first few years to not consider model adjustment processes) the warmer inflow water normally leads to deeper warm isotherms, and vice versa. The warmer (colder) Barents Sea lost more (less) heat during the subsequent cold season (compare green and red lines). If the Barents Sea inflow is high (black line), so the averaged sea temperature will be higher in the next year (due to accumulation heat from the North Atlantic), while its low value results in more cooling conditions in the current year. It is in agreement with above mentioned positive correlation between the

OSD
9, 2121–2151, 2012

averaged for the period of April–March Barents Sea inflow and the top 200 m averaged Barents Sea temperature time series (0.9).

6 Summary and discussion

We have analysed model results from ORCA1 (1°) and ORCA025 (1/4°) NEMO models for the Barents Sea and have found that model results are in agreement with observation data in the Barents Sea along a meridian of 33°30′ E between 70°30′ and 72°30′ N showing negative correlation between ENSO events and water temperature in the Barents Sea. During (or shortly after) the strong warm ENSO event the annual mean ORCA025 model temperature in the Barents Sea decreases by about 0.8 °C and resulting also in a higher sea ice volume. While for cold ENSO events the model shows a lower sea ice volume, and higher annual mean water temperature in the Barents Sea of about 0.7 °C. These values are in a good agreement with observed data (Byshev, 2003). ORCA1 model with coarse resolution (experiments CTL1 and ASSIM1) overestimates the annual Barents Sea inflow about 0.5 Sv (due to not adequate resolution of Faeroe-Scotland channel). So, value 0.5 Sv is more than 1.5 times greater than the value of interannual model variability obtained in all runs (it is about 0.3 Sv) and it is about half of the seasonal variability of the Barents Sea inflow (according to UR025.3 experiment). As a result, there is the overestimation of the contribution of the Barents Sea heat inflow from the North Atlantic to the total heat balance in the Barents Sea. ASSIM1 heat transported from the North Atlantic is about 2 TWt higher compared to UR025.3: it is more than 20 % from interannual UR025.3 variability (that is about 9 TWt). Therefore annual mean water temperature in the Barents Sea obtained in CTL1 and ASSIM1 is respectively about 0.8 °C and more than 1 °C higher than in UR025.3. Nevertheless, the interannual variability of the inflow and annual temperature in all three runs are comparable. All runs give values for warming during cold ENSO events close to observation.

OSD
9, 2121–2151, 2012

It is shown that the Barents Sea inflow is the main source of the Barents Sea heat content variability. During the period of April–July the heat transported from the North Atlantic can be accumulated by the Barents Sea water resulting in the formation of either positive or negative summer heat content anomalies (depending on ENSO events or the type of the previous interaction between the atmosphere and the Barents Sea water) that can influence the state of the Barents Sea during the following cold season. Though during some years, about 30 % of all model cases, effects of heat-exchange with atmosphere can be dominant mechanism in an annual heat balance of the Barents Sea. This exchange can substantially depend upon ENSO events occurring in the preceding years.

Correlation analysis shows that during warm (cold) ENSO events due to global atmospheric teleconnections in April–July higher (lower) atmospheric pressure over the Arctic and atmospheric depression (higher sea level pressure) over the Western Europe are settled. These changes in the atmospheric pressure substantially influence the westerly winds in the North Atlantic that in turn change the Barents Sea inflow. According to the value of correlation coefficient more than 60 % of the Barents Sea inflow variability is explained by the sea level pressure differences between Western Europe and Spitsbergen.

Acknowledgements. This work was supported by the NCEO and the RAPID-Watch Valor projects.

OSD
9, 2121–2151, 2012

References

Adcroft, A., Hill, C., and Marshall, J.: Representation of topography by shaved cells in a height coordinate ocean model, Mon. Weather Rev., 125, 2293–2315, 1997.

Balmaseda, M. A., Vidard, A., and Anderson, D. L. T.: The ECMWF ocean analysis system: ORAS3, Mon. Weather Rev., 136, 3018–3034, doi:10.1175/2008MWR2433.1, 2008.

Barnier, B. and the DRAKKAR Group: Eddy-permitting ocean circulation hindcasts of past decades, Clivar Exchanges, 12, 8–10, 2007.

Barnier, B., Madec, G., Penduff, T., Molines, J. M., Treguier, A. M., Le Sommer, J., Beckmann, A., Biastoch, A., Böning, C., Dengg, J., Derval, J., Durand, E., Gulev, S., Remy, E., Talandier, C., Theetten, S., Maltrud, M., McClean, J., and De Cuevas, B.: Impact of partial steps and momentum advection schemes in a global ocean circulation model at eddy-permitting resolution, Ocean Dynam., 56(5–6), 543–567, doi:10.1007/s10236-006-0082-1, 2006.

Blanke, B. and Delecluse, P.: Variability of the Tropical Atlantic Ocean Simulated by a General Circulation Model with Two Different Mixed-Layer Physics, J. Phys. Oc., 23, 1363–1388, 1993.

Bloom, S. C., Tacks, L. L., daSilva, A. M., and Ledvina, D.: Data assimilation using incremental analysis updates, Mon. Weather Rev., 124, 1256–1271, 1996.

Boyer, T. P., Garcia, H. E., Johnson, D. R., Locarnini, R. A., Mishonov, A. V., Pitcher, M. T., Baranova, O. K., and Smolyar, I. V.: World Ocean Database 2005, NOAA Atlas NESDIS 60, edited by: Levitus, S., 190pp., US Gov. Print. Off., Washington D.C., 2006.

Brodeau, L., Barnier, B., Penduff, T., Treguier, A.-M., and Gulev, S.: An ERA40 based atmospheric forcing for global ocean circulation models, Ocean Model., 31, 88–104, 2010.

Byshev, V. I.: Synoptical and large-scale variability of ocean and the atmosphere, Moscow, Nauka, 343pp., 2003 (in Russian).

Carton, J. A., Chepurin, G., Cao, X., and Giese, B.: A simple ocean data assimilation analysis of the global upper ocean 1950–95. Part I: Methodology, J. Phys. Oceanogr., 30, 294–309, 2000.

Dee, D. P. and Uppala, S.: Variational bias correction of satellite radiance data in the ERA-Interim reanalysis, Q. J. Roy. Meteor. Soc., 135, 1830–1841, 2009.

Dickson, R., Osborn, T., Hurrell, J., Meincke, J., Blindheim, J., Ådlandsvik, B., Vinje, T., Alekseev, G., and Maslowski, W.: The Arctic Ocean Response to the North Atlantic Oscillation, J. Climate, 13, 2671–2696, 2000.

OSD
9, 2121–2151, 2012

Fichefet, T. and Maqueda, M.: Sensitivity of a global sea ice model to the treatment of ice thermodynamics and dynamics, J. Geophys. Res., 102, 12609–12646, 1997.
Furevik, T.: Annual and interannual variability of Atlantic Water temperatures in the Norwegian Seas: 1980–1996, Deep-Sea Res., 48, 383–404, 2001.
Gent, P. R. and McWilliams, J. C.: Isopycnal Mixing in Ocean Circulation Models, J. Phys. Oceanogr., 20, 150–155, 1990.
Goose, H. and Fichefet, T.: Importance of ice-ocean interactions for the global ocean circulation: A model study, J. Geophys. Res., 104, 23337–23355, 1999.
Haines, K., Blower, J., Drecourt, J. P., Liu, C., Vidard, A., Astin, I., and Zhou, X.: Salinity assimilation using S(T) relationships, Mon. Weather Rev., 134, 759–771, 2006.
Haines, K., Valdivieso, M., Zuo, H., and Stepanov, V. N.: Transports and budgets in a 1/4° global ocean reanalysis 1989–2010, Ocean Sci. Discuss., 9, 261–290, doi:10.5194/osd-9-261-2012, 2012.
Harms, I., Schrum, C., and Hatten, K.: Numerical sensitivity studies on the variability of climate-relevant processes in the Barents Sea, J. Geophys. Res., 110, C06002, doi:10.1029/2004JC002559, 2005.
Hughes C. W. and Stepanov, V. N.: Ocean dynamics associated with rapid J2 fluctuations: Importance of circumpolar modes and identification of a coherent Arctic mode, J. Geophys. Res., 109, C06002, doi:10.1029/2003JC002176, 2004.
Ingleby, B. and Huddleston, M.: Quality control of ocean temperature and salinity profiles – Historical and real-time data, J. Marine Syst., 65, 158–175, 2007.
Large, W. G. and Yeager, S. G.: Diurnal to decadal global forcing for ocean and sea-ice models: The data sets and flux climatologies, Technical Report TN-460+STR, NCAR, 105pp., 2004.
Lique, C., Treguier, A. M., Scheinert, M., and Penduff, T.: A model-based study of ice and freshwater transport variability along both sides of Greenland, Clim. Dynam., 33, 685–705, doi:10.1007/s00382-008-0510-7, 2009.
Lique, C., Treguier, A. M., Blanke, B., and Grima, N.: On the origins of water masses exported along both sides of Greenland: a Lagrangian model analysis, J. Geophys. Res., 115, C05019, doi:10.1029/2009JC005316, 2010.
Loeng, H., Ozhigin, V., and Ådlandsvik, B.: Water fluxes through the Barents Sea, ICES J. Mar. Sci., 54, 310–317, 1997.

OSD
9, 2121–2151, 2012

Madec, G.: NEMO reference manual, ocean dynamics component: NEMO-OPA, Preliminary version, Note du Pole de modélisation, Institut Pierre-Simon Laplace (IPSL), France, No. 27, ISSN 1288-1619, 2008.
Madec, G., Delecluse, P., Imbard, M., and Levy, C.: OPA 8.1 general circulation model reference manual, Notes de l'IPSL, University P. et M. Curie, B102 T15-E5, Paris, No. 11, 91pp., 1998.
Penduff, T., Le Sommer, J., Barnier, B., Treguier, A.-M., Molines, J.-M., and Madec, G.: Influence of numerical schemes on current-topography interactions in 1/4° global ocean simulations, Ocean Sci., 3, 509–524, doi:10.5194/os-3-509-2007, 2007.
Penduff, T., Juza, M., Brodeau, L., Smith, G. C., Barnier, B., Molines, J.-M., Treguier, A.-M., and Madec, G.: Impact of global ocean model resolution on sea-level variability with emphasis on interannual time scales, Ocean Sci., 6, 269–284, doi:10.5194/os-6-269-2010, 2010.
Roullet, G. and Madec, G.: Salt conservation, free surface, and varying levels: a new formulation for ocean general circulation models, J. Geophys. Res., 105, 23927–23942, 2000.
Serreze, M., Barrett, A., Slater, A., Steele, M., Zhang, J., and Trenberth, K.: The large-scale energy budget of the Arctic, J. Geophys. Res., 112, D11122, doi:10.1029/2006JD008230, 2007.
Simmons, A., Uppala, S., Dee, D., and Kobayashi, S.: ERA-Interim: New ECMWF reanalysis products from 1989 onwards, ECMWF Newsletter, 110, 25–35, 2007.
Smedsrud, L. H., Ingvaldsen, R., Nilsen, J. E. Ø., and Skagseth, Ø.: Heat in the Barents Sea: transport, storage, and surface fluxes, Ocean Sci., 6, 219–234, doi:10.5194/os-6-219-2010, 2010.
Smith, G. C. and Haines, K.: Evaluation of the S(T) assimilation method with the Argo dataset, Q. J. Roy. Meteor. Soc., 135, 739–756, 2009.
Troccoli, A. and Haines, K.: Use of the temperature-salinity relation in a data assimilation context, J. Atmos. Ocean. Tech., 16, 2011–2025, 1999.
Tsubouchi, T., Bacon, S., Naveira Garabato, A. C., Aksenov, Y., Laxon, S., Fahrbach, E., Beszczynska-Möller, A., Hansen, E., Lee, C. M., and Ingvaldsen, R. B.: The Arctic Ocean in summer: boundary fluxes and water mass transformation, J. Geophys. Res., 117, C01024, doi:10.1029/2011JC007174, 2012.

OSD
9, 2121–2151, 2012

Table 1. A description of experiments.

No	Experiment	Description
1	CTL1	Control simulation forced with ERAInterim and initialised from 1989 from WOA05 climatology (ORCA1 model)
2	ASSIM1	Initialised and forced as CTL1 but with EN3 data assimilation (ORCA1 model)
3	UR025.3	Control 1/4° NEMO simulation forced with ERAInterim and initialised in Jan 1989 from EN3 in situ data assimilation experiment started in 1958 and driven by DFS3 forcings

OSD
9, 2121–2151, 2012

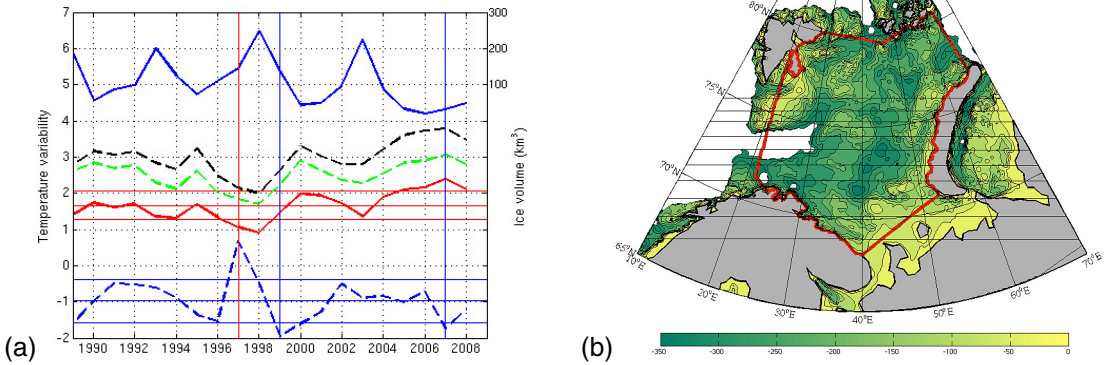

Fig. 1. (a) Annual top 200 m averaged temperature from CTL1 (dashed green), ASSIM1 (dashed black) and UR025.3 (red), and annual UR025.3 sea ice volume (blue) in the Barents Sea. NINO3-index is shown by dashed blue line. Vertical lines show the beginning of onsets of warm (red) and cold (blue) ENSO events and horizontal lines – mean values plus and minus standard deviations (for curves corresponding to the same colours); **(b)** The region of the Barents Sea used for calculation of mean values.

OSD
9, 2121–2151, 2012

The link between the Barents Sea and ENSO events

V. N. Stepanov et al.

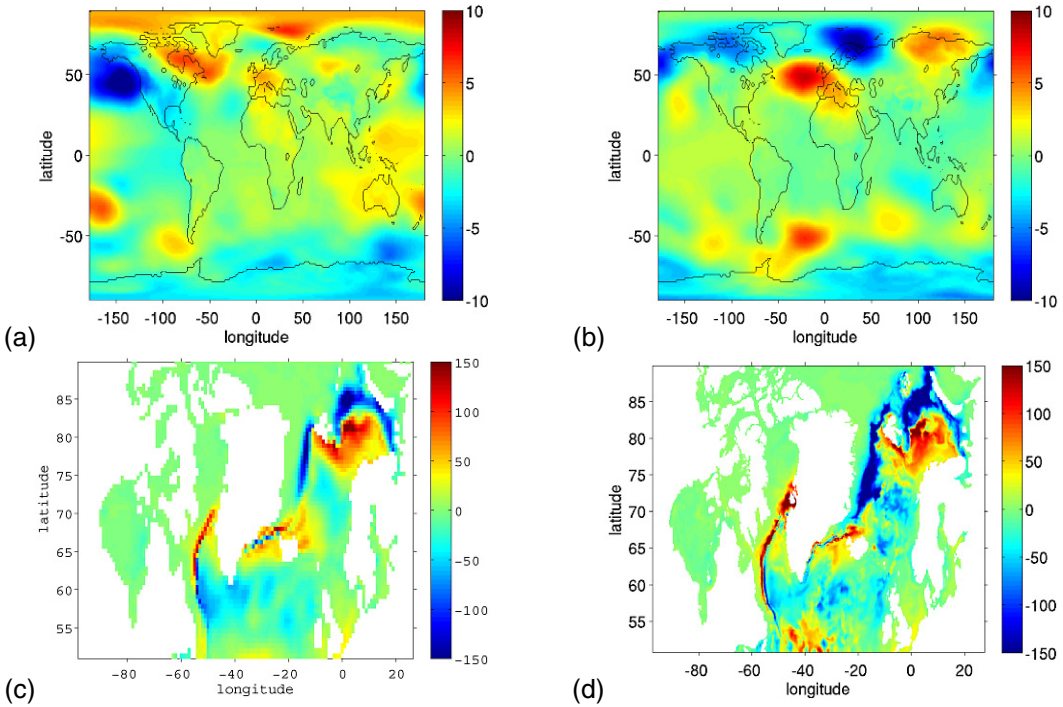

Fig. 2. Sea level pressure anomaly (in HPa) for January–March of 1998 **(a)** and 2000 **(b)** after onsets of warm and cold ENSO events, respectively; net surface heat flux difference (in $W\,m^{-2}$) between 2000 and 1998 averaged for January–March period according to CTL1 **(c)** and UR025.3 **(d)** runs.

OSD
9, 2121–2151, 2012

The link between the Barents Sea and ENSO events

V. N. Stepanov et al.

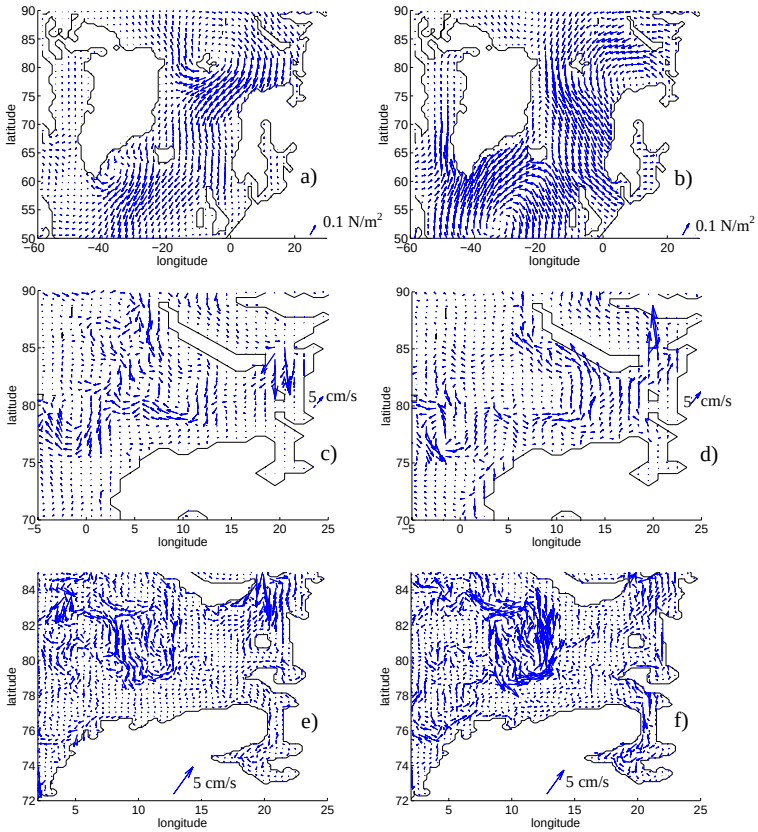

Fig. 3. Wind stress anomaly (for the period 1989–2008) over the North Atlantic and the Barents Sea **(a, b)** and the top 200 m averaged velocity anomaly in the Barents Sea (**c, d** – experiment CTL1; **e, f** – UR025.3 run) for January–March of 1998 **(a, c, e)** and 2000 **(b, d, f)** after warm and cold ENSO events, respectively.

OSD
9, 2121–2151, 2012

The link between the Barents Sea and ENSO events

V. N. Stepanov et al.

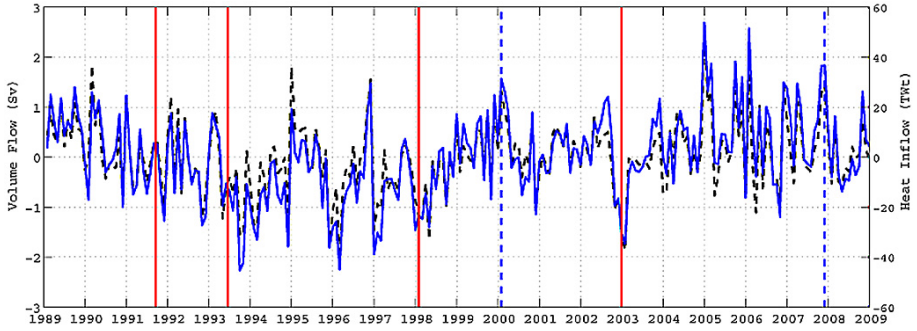

Fig. 4. Monthly UR025.3 anomalies of volume (dashed black line) and heat inflow into the Barents Sea (solid blue line) after removing seasonal cycle. Vertical lines show correspondence between warm (solid red) and cold (dashed blue) ENSO events and variability of heat transport into the Barents Sea from the North Atlantic.

OSD
9, 2121–2151, 2012

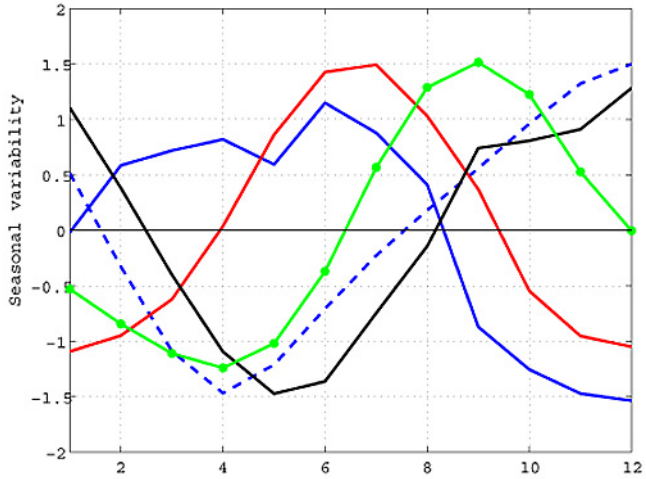

Fig. 5. Normalized seasonal cycle (to have zero mean and a standard deviation of one) of the depth of 1 °C isotherm (blue, 261 ± 79 m), the minimal temperature value in the deep 130–320 m layer (dashed blue, 1.48 ± 0.40 °C); the top 200 m averaged Barents Sea temperature (green, 1.66 ± 0.95 °C), the Barents Sea heat inflow (black, 86.5 ± 21.0 TW) and the net surface flux (red, −98.6 ± 158.8 W m^{-2}). The mean and standard deviation values are given in square brackets.

OSD
9, 2121–2151, 2012

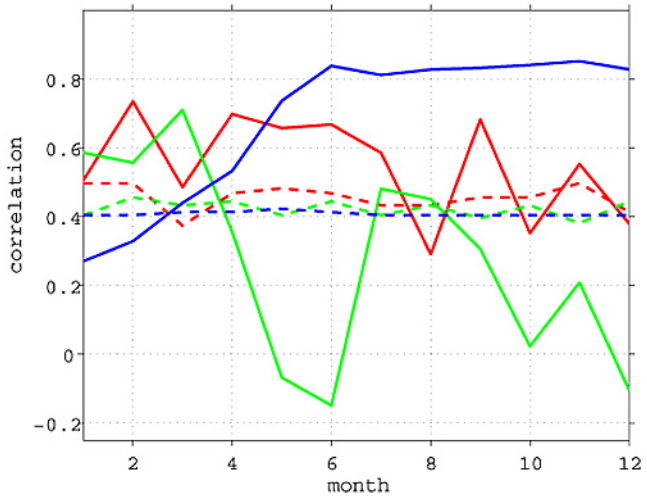

Fig. 6. Correlations annual NINO3-index (blue), the heat due to the Barents Sea inflow (red) and net surface heat flux (green) time series with their time series corresponding to each month; dashed lines denote corresponding statistical significance at the 95 % level.

OSD
9, 2121–2151, 2012

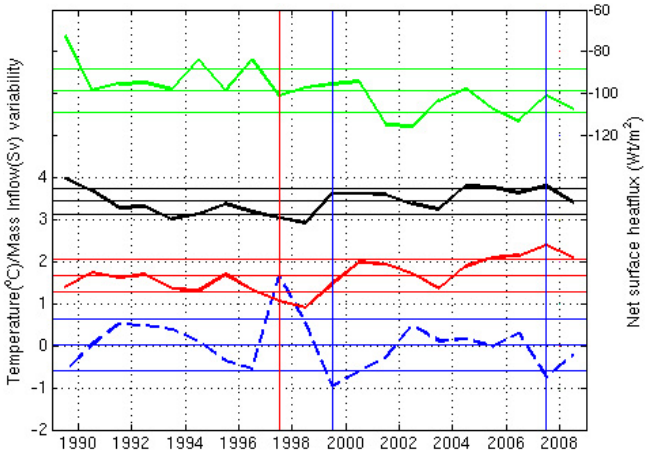

Fig. 7. Annual top 200 m averaged temperature (red) together with the Barents Sea inflow (black line) and net surface heat loss (green) from UR025.3 experiment. NINO3-index is shown by dashed blue line. Vertical lines show warm (red) and cold (blue) ENSO events and horizontal lines – plus and minus standard deviations (for curves corresponding to the same colours).

OSD
9, 2121–2151, 2012

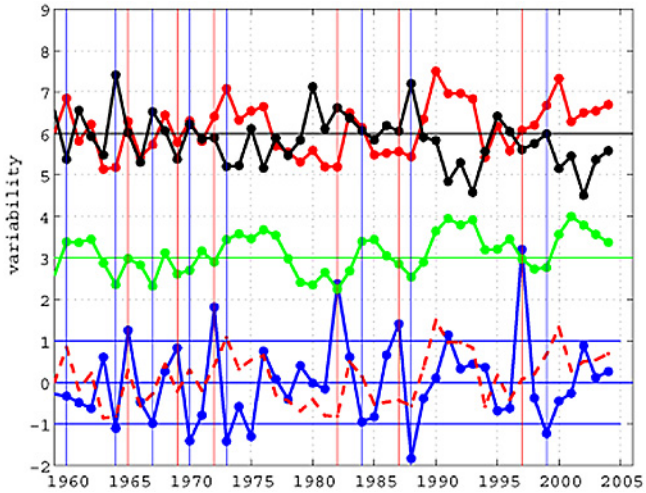

Fig. 8. Normalized April–December (for current year) mean time series of NINO3-index (blue); April/a current year–March/a subsequent year mean of the Barents Sea heat inflow (red), the net surface flux (black) and the averaged on the Barents Sea heat content (green) from ORCA025-G70 run. Details see in the text. Vertical lines show maxima (red) and minima (blue) NINO3-index (more its standard deviation, thin blue horizontal lines).

OSD
9, 2121–2151, 2012

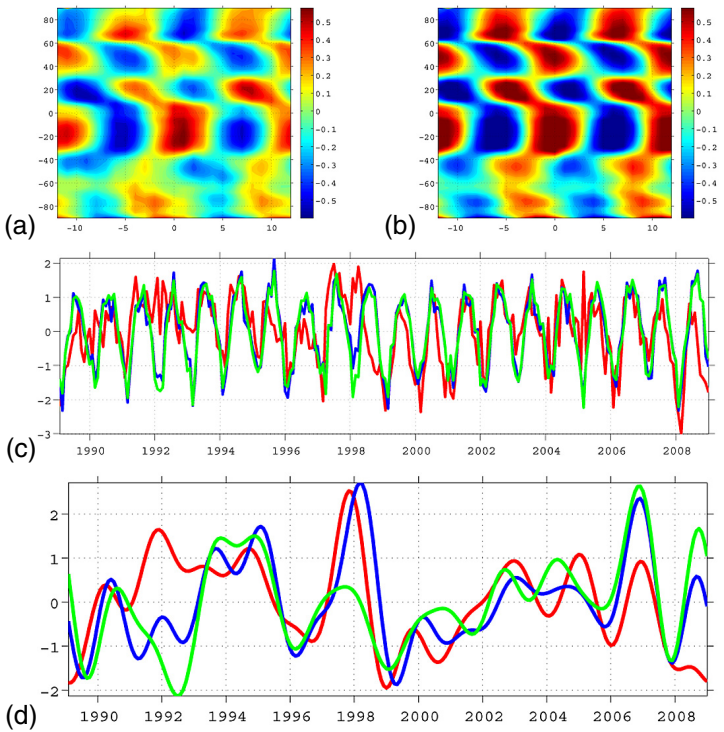

Fig. 9. 1989–2008 correlations of zonally averaged sea level pressure with SOI-index with negative signs **(a)**, and **(b)** with the zonally averaged sea level pressure difference between 17° and 12° S. Positive lags means that the zonally averaged sea level pressure lags from corresponding time series. **(c)** time series of SOI-index with negative signs (red), zonally averaged sea level pressure difference between 17° and 12° S (blue), and zonally averaged sea level pressure difference between 17° and the equator (green); **(d)** the same as **(c)** but the seasonal cycle was removed and low-pass filtering with periods longer than 18 months was applied.

OSD
9, 2121–2151, 2012

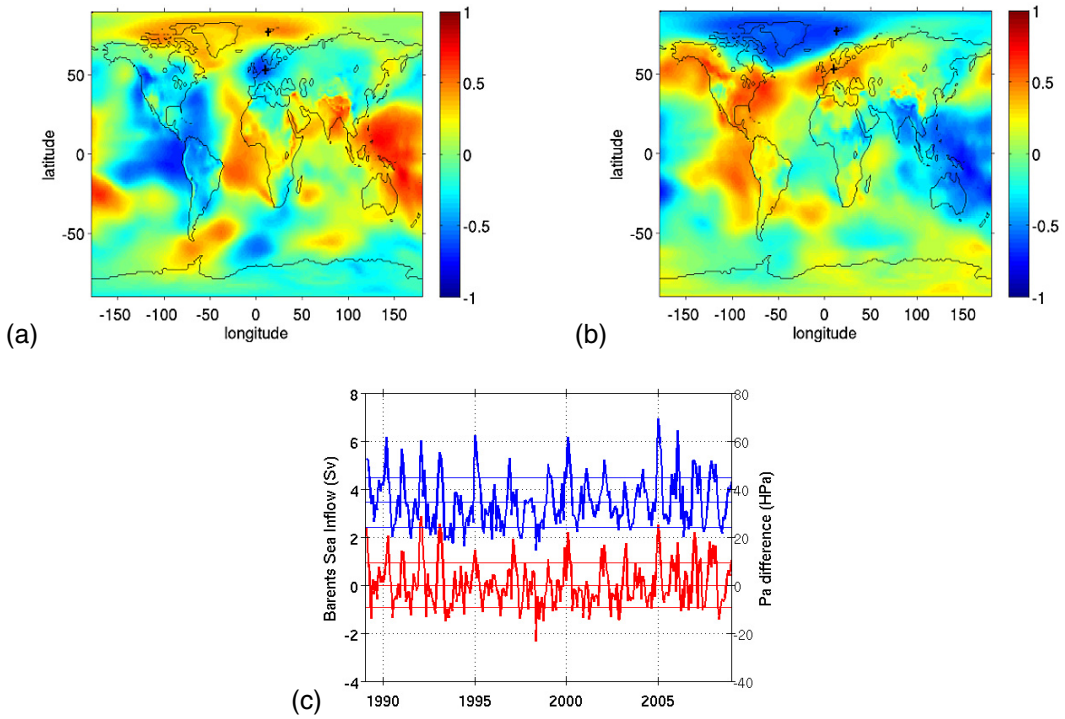

Fig. 10. 1989–2008 correlations of mean sea level pressure averaged for the period from April to July with April NINO3-index **(a)** and **(b)** with the averaged for the same period Barents Sea inflow; **(c)** the Barents Sea inflow (blue) and (red) pressure differences between Western Europe and Spitsbergen (the regions are marked by black crosses on Fig. 9a–b).

OSD
9, 2121–2151, 2012

The link between the Barents Sea and ENSO events

V. N. Stepanov et al.

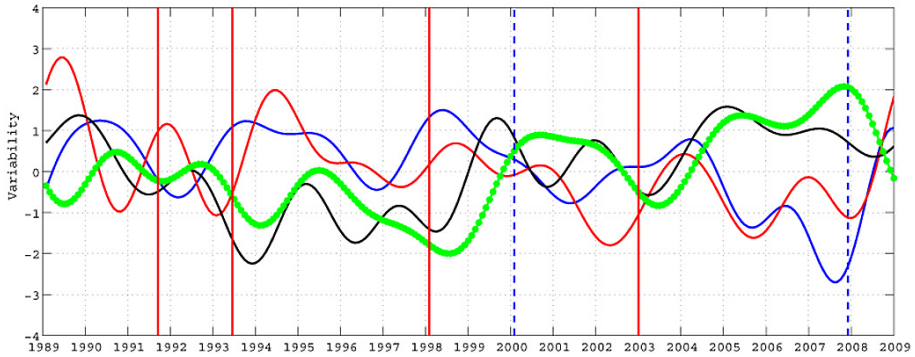

Fig. 11. Normalized on their standard deviations anomalies (after subtraction of seasonal cycle) of the depth of 1 °C isotherm (blue), the top 200 m averaged Barents Sea temperature (green), the Barents Sea heat inflow (black) and the net surface flux (red).

OSD
9, 2121–2151, 2012